Check for updates

Synthesis of hierarchically mesoporous silica with encapsulated avobenzone as a UV protection filter

Wei-Hsun Wang,†[abcd] Hsin-Tung Liang,†[e] Yuan-Ting Yang-Wang[e] and Chi-Jen Shih [ID] *[efg]

In this study, hierarchically mesoporous silica (HMS) with properties such as high specific surface area, high photostability, and no cellular toxicity was synthesized. The synthesized silica can be considered as an excellent carrier candidate material. Through the use of nitrogen adsorption and desorption analysis, the shape of the hysteresis loop implied the presence of mesoporous structures in the HMS powder. In addition, the encapsulation efficiency was more than 90%. These results showed that avobenzone could be encapsulated into the HMS powder because of its high specific surface area and pore volume. Additionally, X-ray diffractometry (XRD), Fourier transform infrared spectroscopy (FTIR), thermal gravimetric analysis (TGA), and UV-visible (Vis) spectrophotometry were used to prove that the hierarchically mesoporous silica was able to effectively encapsulate avobenzone. In addition, the new synthetic sunscreen kept its excellent UVA absorption properties after being encapsulated.

Introduction

Solar ultraviolet (UV) radiation is known to harm human skin and cause issues such as melanoma, inflammation, photo-aging, and cancer.[1–4] In addition, immunosuppression and DNA damage can occur from UV radiation exposure.[5,6] UV light is divided into three types: UVA, UVB, and UVC. UVA (320–400 nm) can penetrate the epidermis layer to the dermis layer, leading to a photosensitive reaction *via* free radicals.[7] Thus, according to several previous studies, exposure to UV radiation can be limited by using sunscreen products, thereby reducing the risk of skin cancers such as basal-cell carcinoma (BCC) and squamous-cell carcinoma (SCC).[8–10]

Avobenzone is one of the few organic UVA filters that is widely used in broad-spectrum sunscreen products.[11] The absorption spectra of avobenzone ranges from 320 to 400 nm with peak absorption at around 355 nm.[12] However, the photochemical reactions of avobenzone have already been thoroughly researched. Aryl glyoxal and benzoic acid are the main products from photo-degraded avobenzone.[13] The photo-degradation products cause a reduction in UV protection ability and destabilize the sunscreen product. Avobenzone under UV light has a very poor light-stability. Avobenzone has a strong absorption in the UVA range at 360 nm but is rapidly destroyed after irradiation.[14] Due to avobenzone isomerized when submitted to UV light.[15] Furthermore, these harmful photo-degradation products from avobenzone penetrate into the skin. A high concentration of these products can cause skin irritation, biological accumulation, photosensitive dermatitis, and contact dermatitis.[14,16]

To reduce these shortcomings, there are and increasing number of studies associated with UV filters that have focused on methods related to encapsulation and incorporation to diminish the damage to human skin.[17,18] There have been many reports that different materials can be used as photoprotective agents to prevent human skin from UV filter damage.[19–22] Wu *et al.* demonstrated that using polymethyl methacrylate (PMMA) to encapsulate organic UV filters improved their safety, photo-protectivity, and photostability.[19] Cabrera *et al.* found that liposheres are highly loaded and under a narrow particle distribution obtained from carnauba wax. Avobenzone was encapsulated into liposheres to enhance its photostability after the encapsulation process.[20] Scalia *et al.* indicated that the encapsulation of avobenzone within hydroxypropyl-β-cyclodextrin provided better protection of UV radiation and decreased the skin penetrability of avobenzone.[21] The disadvantages of those carrier materials, including thermal instability, pH instability, and potential reduced complexation efficacy, was also studied.[23–25]

[a]Department of Orthopedic Surgery, Changhua Christian Hospital, Changhua, Taiwan

[b]School of Medicine, Kaohsiung Medical University, Kaohsiung, Taiwan

[c]Department of Medical Imaging and Radiology, Shu-Zen Junior College of Medicine and Management, Kaohsiung, Taiwan

[d]Department of Golden-Ager Industry Management, Chaoyang University of Technology, Taichung, Taiwan

[e]Department of Fragrance and Cosmetic Science, College of Pharmacy, Kaohsiung Medical University, 100 Shi-Chuan 1st Road, Kaohsiung 80708, Taiwan. E-mail: cjshih@gap.kmu.edu.tw; Tel: +886 73121101 ext. 2367

[f]Department of Medical Research, Kaohsiung Medical University Hospital, Kaohsiung, Taiwan

[g]Drug Development and Value Creation Research Center, Kaohsiung Medical University, Taiwan

† These authors contributed equally to this work.

Hierarchically mesoporous silica (HMS) with ordered pore structures ranging from 2 nm to 50 nm at multiple length scales is one potential carrier material and is derived from the evaporation-induced self-assembly (EISA) method.[26] In addition, it is an inorganic oxide, having a high encapsulated volume, great temperature and pH resistance, and no photocatalysis. An extremely low degradation rate and the controlled release effect are the distinguishing features of this material.[27–30] Moreover, HMS has high photostability and UV protective effects. Many studies indicated that hierarchically mesoporous silica could be utilized as a great carrier and improve the shortage of the origin materials.[31–33]

Compared with the above, the contribution and novelty of this study are list in the following three points:

(1) To provide a preparing method for mesoporous silica to effectively encapsulate with avobenzone.

(2) The test samples formed by the above preparing method used Fourier transform infrared (FTIR) spectroscopy and X-ray diffractometer (XRD) for qualitative analysis, and Brunauer–Emmett–Teller (BET) method and thermogravimetric analyzer (TGA) for quantitative analysis to verify the encapsulation efficiency was more than 90%.

(3) The resulting avobenzone encapsulated powder kept its excellent UVA absorption abilities.

Materials and methods

Sources of raw materials

Tetraethyl orthosilicate (TEOS) (ACROS, 98%) was used as a silica precursor. Pluronic F-127 (BASF) was used as a non-ionic surfactant. 2 M nitric acid (SHOWA, 98%) was used as catalyst for the hydrolysis reaction. Ethanol (J. T. Baker, 99.9%) was used as a solvent to mix all ingredients of the HMS. Polyurethane foam (PUF) was used as a scaffold for the HMS. Acetone (Seedchem, 98.5%) was used as a solvent to dissolve the avobenzone. Avobenzone (Essence Plus) was used as the encapsulated material in the HMS. All chemicals were of analytical reagent grade and were used without any further purification.

Material preparation

Following the EISA method,[26] the experimental materials for HMS were prepared using polyurethane foam (PUF) and the non-ionic surfactant F127 as the pore-forming agents.

TEOS, 2 M nitric acid, and non-ionic surfactant F127 were dissolved and mixed together in anhydrous ethanol. Then, the mixture was stirred at room temperature for 24 h to form a solution. Next, the PUFs were soaked in the mixture and dried in an oven at 100 °C for 1 d. After the PUFs were fully dried, they were heated in a tube furnace from room temperature to the calcination temperature of 550 °C at a constant heating rate of 2 °C min^{-1} and were held at the calcination temperature for 4 h to remove the forming agents and impurities. The powders were ground after cooling and sieved through #325 meshes.

Avobenzone encapsulation

The avobenzone encapsulated powder was prepared according to the physical adsorption principle.[34] In the experiment, acetone was the solvent used to dissolve the avobenzone. Next, the HMS was mixed with the solution that also contained the acetone and avobenzone. Afterwards, the mixture was stirred at room temperature for 24 h. Finally, the acetone was removed using a rotary evaporator. The resulting avobenzone encapsulated powder is referred to as MSAB. MSAB was a combination of HMS powders per unit area with different weights of avobenzone respectively 0.98 mg m^{-2}, 1.95 mg m^{-2} and 2.93 mg m^{-2}, which were named MSAB-0.98 mg m^{-2}, MSAB-1.95 mg m^{-2}, and MSAB-2.93 mg m^{-2}. This notation was to highlight that the specific surface area was an important factor in evaluating the loading capacity. 0.98 mg m^{-2}, 1.95 mg m^{-2} and 2.93 mg m^{-2} were obtained by 0.5 g, 1 g, and 1.5 g of the encapsulated avobenzone weight dividing by the specific surface area (511.6 m^2) of mesoporous silica, respectively.

Textural characterization of MSAB

The Quantachrome Autosorb 1 sorption analyzer measured the isotherms of nitrogen adsorption and desorption at 77 K. MSAB-0.98 mg m^{-2} underwent a pretreatment where it was degassed at 150 °C under a high vacuum for 12 h by the degas port of the adsorption analyzer to test the sample before and after avobenzone encapsulation. The instrument (ASAP 2010, Micromeritics, USA) used in this experiment calculated the specific surface areas with the Brunauer–Emmett–Teller (BET) method and the Barret–Joyner–Halenda (BJH) equation. Nitrogen gas was used as the adsorbent.

Characterization

The FTIR absorption spectra were analyzed using a spectrometer (Nicolet 6700, Thermo, USA). Before and after avobenzone encapsulation, the MSAB powder samples were mixed with particles of potassium bromide (KBr) (the mass ratio of the sample to KBr was 1 : 10) and pressed into 200 mg pellets each with a diameter of 12 mm. The infrared absorption spectra were procured in the frequency range of 400–4000 cm^{-1} for the spectrum. The composite spectrum for all samples took an average of 32 scans. Otherwise, each sample in this experiment was normalized to the spectrum of a blank KBr pellet.

The X-ray diffraction (XRD) patterns characterized the phase composition of different ratios of MSAB before and after avobenzone encapsulation. XRD was performed using an X-ray diffractometer (XRD-6000, Shimadzu, Japan). The diffracted intensity of Cu Kα radiation ($\lambda = 1.5418$ Å) was measured in a 2θ range between 10° and 80° with a step size of 4° min^{-1}. The scans were recorded at 30 kV and 20 mA.

In addition, transmission electron microscopy (TEM) images were recorded using the microscopy (JEM-2100, JEOL, Japan). The MSAB powder samples were dispersed in distilled-deionized water using an ultrasonicator, which shocked the samples. Then, the samples were dropped onto a copper grid, evaporating the solvent.

Before and after avobenzone encapsulation, the thermal decomposition of HMS, MSAB-0.98 mg m^{-2}, and avobenzone were obtained using an analyzer (TA-Thermogravimetry & Differential Thermal Analysis 300, Mettler-Toledo, USA). Thermogravimetric analyses (TGA) were recorded while raising the temperature from 30 °C to 800 °C under a heating rate of 10 °C min^{-1} in air.

UV-vis absorption spectra were examined using a spectrometer (DU 730, Beckman Coulter, USA). In addition, the UV-vis spectrophotometer was used to record absorption spectra at room temperature in the wavelength range of 200–800 nm.

Result and discussion

Texture of MSAB powders

The nitrogen adsorption–desorption analysis characterized MSAB powders before and after the avobenzone encapsulation. As shown in Fig. 1(a), the MSAB adsorption–desorption curves were determined. The formation of the hysteresis curves for the HMS were compared with H1 patterns of type IV at high relative pressure between 0.8 and 1.0,[35] and pore size distribution shown in Fig. 1(b). For the HMS powder, the shape of this hysteresis loop implies the presence of mesoporous structures.[36] Additionally, the hysteresis curves after avobenzone encapsulation, which are shown in Fig. 2, indicate that the texture was not destroyed by the encapsulated avobenzone. In Table 1, the specific surface areas and the mesoporous volume properties of the HMS and MSAB samples were presented. The
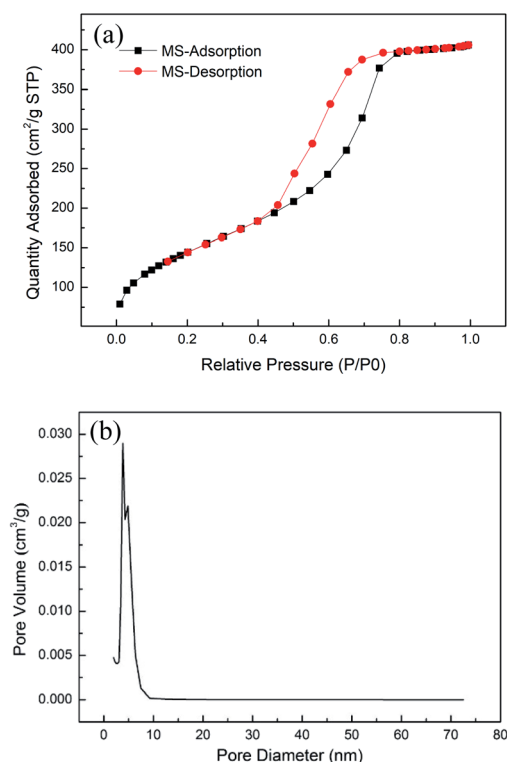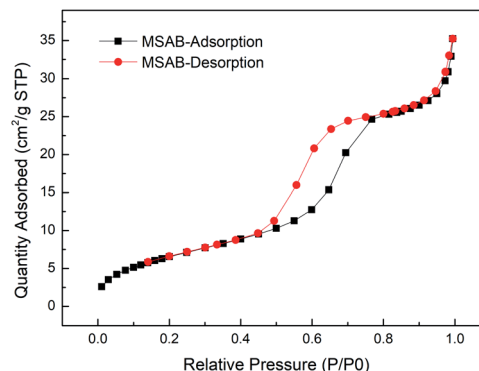

Fig. 2 Nitrogen adsorption and desorption isotherms of MSAB powders.

specific surface areas of the HMS have an average of 511.6 m^2 g^{-1}, and the pore volume of mesopores are around 0.63 cm^3 g^{-1}. The formation of the HMS signified that the material has a high specific surface area and porous structure. In previous reports, the specific surface areas range of mesoporous silica are about 535–787 m^2 g^{-1}, the pore size range of mesopores are about 2.1–15 nm, and the pore volume of mesopores are about 0.68–1.17 cm^3 g^{-1}.[37,38] In addition to the difference in the manufacturing process, the type of template surfactant (e.g. F-127 or P123) selected will also cause the mesopore size to be different. Using a PUF template different from the conventional method and a higher heat treatment temperature of 600 °C in this study, so the specific surface areas and the pore volume of mesoporous silica are smaller slightly compared with the previous reports.

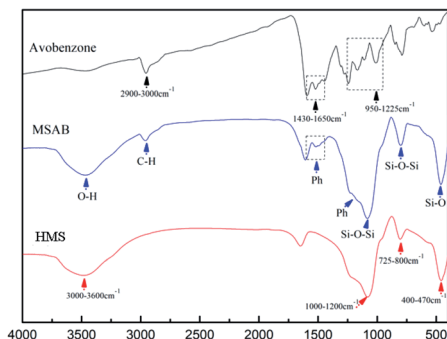### Evaluation of avobenzone encapsulation

Li et al. demonstrated how to analyze mesoporous silica aerogel after UV filter encapsulation results from a FTIR spectra.[39] The analysis of the FTIR was used to identify the coupled surface vibrations of the prepared MSAB in the powder samples. The FT-IR spectra patterns, shown in Fig. 3, for the HMS powders discovered organic bond vibrations at 725–800 cm^{-1} and 1000–1200 cm^{-1} for Si–O–Si, 400–470 cm^{-1} for Si–O, and 3000–3600 cm^{-1} for O–H.

In addition to the bonding of the HMS powders after avobenzone encapsulation, there were C–H framework vibrations in the FTIR spectra patterns of the avobenzone absorption bands at 2900–3000 cm^{-1}. The absorption bands that represent the stretching vibration of the benzene ring and C–H in-plane bending vibration, as shown in Fig. 3, and assignment of characteristic bands shown in Table 2, are at 1430–1650 cm^{-1} and 950–1225 cm^{-1}, respectively.[40] Additionally, characteristic bands of avobenzone in MSAB did not shift, implying that avobenzone was encapsulated into the HMS without chemical bonding. This result signified that the HMS samples with encapsulated avobenzone were successfully bonded.

The XRD patterns of HMS, MSAB-0.98 mg m^{-2}, MSAB-1.95 mg m^{-2}, and MSAB-2.93 mg m^{-2} were shown in Fig. 4. The HMS used in the experiments did not demonstrate any obvious characteristic peaks. This showed that the HMS was in the

Fig. 1 (a) Nitrogen adsorption and desorption isotherms of MS powder and (b) pore size distribution.

Table 1 The BET surface area and pore volume of HMS powders before and after avobenzone encapsulation

	S_{BET} before encapsulating $(m^2\ g^{-1})$	S_{BET} after encapsulating $(m^2\ g^{-1})$	The percentages of decrease S_{BET} (%)	V_p before encapsulating $(cm^3\ g^{-1})$	V_p after encapsulating $(cm^3\ g^{-1})$	The percentages of decrease V_p (%)
HMS powders	511.6	24.97	95.12	0.63	0.055	91.27

Fig. 3 FTIR spectra of avobenzone, MSAB powders, and HMS powders.

Table 2 Assignment of characteristic bands observed in FTIR spectra of avobenzone, MSAB and HMS samples

Assignment	Band position (cm^{-1})
Si–O	400–470
Si–O–Si	725–800
Si–O–Si	950–1225
Ph	1430–1650
C–H	2900–3000
O–H	3000–3600

amorphous phase and exhibited the same properties as other mesoporous materials.

In contrast, being encapsulated by carriers declined the degree of crystallinity of the MSAB. We speculate that the mesopores of the MSAB did not form the ordered structure of crystalline states, which caused the decrease in degree of crystallinity after avobenzone was encapsulation, based on the XRD analysis. The driving forces of the interactions were ascribed that heterogeneous nucleation and growth by thermodynamics could reduce the surface energy between avobenzone and the HMS. In addition, different amounts of avobenzone were encapsulated into per unit area (m^2) of HMS (0.98 mg, 1.95 mg, and 2.93 mg).
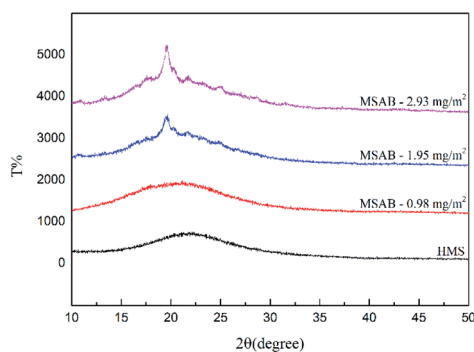
The resulting of XRD avobenzone patterns showed apparent characteristic peaks.[41–43] The results for MSAB in Fig. 4 showed characteristic bands that were similar to prior research.[42] The adsorption between HMS and avobenzone did not affect the XRD patterns of the other powders. In addition, there were no new crystals and only a weak reduction in the relative intensity. The patterns of the XRD analysis also indicated the increase in the degree of crystallinity based on the entrapment yield of the powders. This is because that avobenzone was immobilized on the surface of HMS to suppress the spontaneous crystallization of avobenzone.[44] This evidences that there was a crystallographic plane, and we estimated that the maximum amount of encapsulated avobenzone was approximately 0.98 mg m^{-2}. Only when avobenzone encapsulating in mesopores completely, the situation of MSAB was in the amorphous phase without producing any crystalline. Furthermore, while the quantity of avobenzone exceeded 0.98 mg m^{-2}, some of the avobenzone did not become encapsulated but was mixed with the HMS carrier in the second mixture phase.

To sum up the above results, it indicated that only the mesopores was filled up with avobenzone. There did not show any degree of crystallinity. In addition, we did the cross-comparison with the result of BET. It revealed that the material with high specific surface area could adsorb more avobenzone particles. Simultaneously, the percentages of decrease

Fig. 4 XRD patterns of HMS powders and different ratios of MSAB powders.
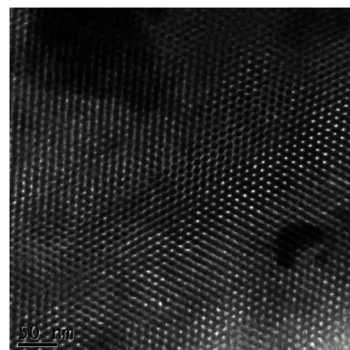
Fig. 5 TEM images of HMS powder after avobenzone encapsulation.

pore volume became much smaller. As a result, we could speculate that the avobenzone powders were encapsulated in the HMS carrier.

Fig. 5 shows that the TEM image of the HMS was regular, interconnected, and had ordered mesopores. In addition, the diameter range of mesopores was approximately 3–5 nm, and average diameter was approximately 4.1 nm ($N = 50$). Furthermore, the TEM image for the MSAB confirmed that one part showed mesopores partially loaded with avobenzone.

By observing the HMS powders before and after avobenzone encapsulation, we can confirm that the specific surface area, pore volume, and pore size of the mesopores decreased after avobenzone encapsulation. It is therefore apparent that avobenzone was encapsulated into the HMS powders successfully. For HMS powders encapsulated into avobenzone, the specific surface area and pore volume declined by 95.12% and 91.27%, respectively, as shown in Table 1. The influence of nitrogen adsorption–desorption measurements could be explained by the avobenzone being absorbed into the mesopores of the HMS powders, and this could also be the reason of why the avobenzone was encapsulated into the mesoporous structures. As previously mentioned, a successful avobenzone encapsulation would result in a reduction in specific surface area and pore volume.

The HMS powders after avobenzone encapsulation were evaluated using TGA. The TGA curve shows the HMS before and after avobenzone encapsulation in Fig. 6. The weight loss of the HMS powders was 3% between 30 °C and 100 °C. This loss could be due to the evaporation of water and ethanol from the HMS powders. The amount of weight loss of avobenzone increased at 250 °C, and avobenzone was completely burned out at 750 °C. HMS, a kind of multi-pore structure material, did not show any obvious change at 800 °C. Based on these results, it is judged that the residual weight of MSAB, of which the ratio between HMS and avobenzone is two to one, is equal to the weight of HMS at 800 °C. The avobenzone encapsulation capacities of HMS were calculated to be 66.31%. This demonstrates that the encapsulation efficiency is extremely high.

In addition, we chose the MSAB avobenzone encapsulated ratio, which is 0.98 mg m^{-2}, to be analyzed, and the results
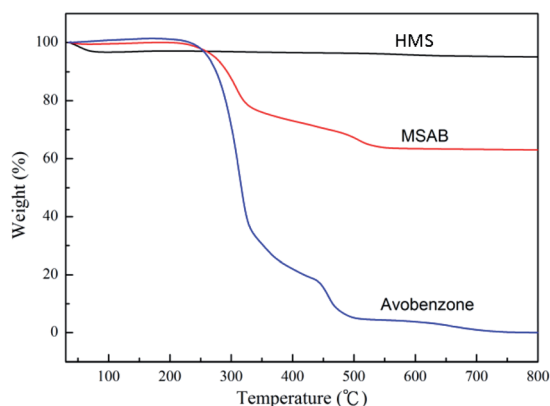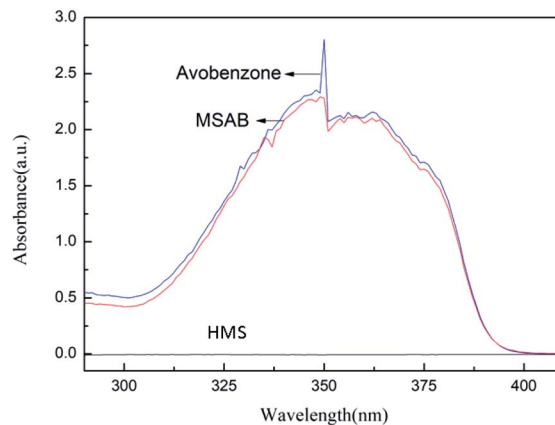

Fig. 7 UV-vis spectra of avobenzone, MSAB powders, and HMS powders.

remained unchanged as compared to the original ratio of HMS to avobenzone.

The UV-protection ability results of the MSAB, the absorbance of HMS, MSAB, and avobenzone, as shown in Fig. 7, were analyzed using the UV-vis absorption spectrophotometer. HMS did not present any characteristic peaks between 200 nm to 800 nm of absorbance. The absorption bands of MSAB are located in the 320–400 nm range, which are the characteristic bands of UVA radiation. In addition, the characteristic peak presented at around 350 nm, which matched the results from previous research.[15] This outcome is identical to the absorbance of avobenzone. As the result, the HMS powders after avobenzone encapsulation still maintained great UV protection abilities.

Conclusions

In this study, three variations of MSAB were prepared by isothermal loading and were applied to an HMS material. Acetone was used as the medium for encapsulating avobenzone into thee HMS through the simple adsorption method. The results of this research are summarized as follows:

(1) The results of nitrogen adsorption–desorption measurements were calculated to characterize HMS before and after avobenzone encapsulation. Mesoporous structures resulted from the high specific surface area. The rate of decreasing specific surface area was 95.12%, and the rate of decreasing pore volume was 91.27%.

(2) According to the XRD patterns of MSAB, the maximum amount of encapsulated avobenzone is 0.98 mg m^{-2}. The avobenzone that exceeded 0.98 mg m^{-2} was not encapsulated into MSAB, but was mixed into the second phase mixture with the HMS carrier.

(3) From the FTIR analysis, it can be confirmed that the HMS powders contained both characteristic peaks of HMS and avobenzone after avobenzone encapsulation. Additionally, the characteristic bands of avobenzone in MSAB did not shift, demonstrating that there was no chemical bond formation between HMS and avobenzone.

Fig. 6 TGA curves of avobenzone, MSAB powders, and HMS powders.

(4) Based on the TGA curves, the ratio of HMS and avo-benzone is two to one in MSAB. The result is the same as the original ratio of HMS to avobenzone. In addition, the avo-benzone encapsulation capacity of MSAB was calculated to be 66.31%.

(5) The TEM images directly indicated that the avobenzone encapsulated into HMS was prepared properly. The diameter range of the mesopores was approximately 3–5 nm.

(6) Based on the results from the UV absorption spectra, MSAB showed the characteristic bands at 320–400 nm with the characteristic peak at around 350 nm, which coincides with the bands of UVA protection. This showed that the HMS powders after avobenzone encapsulation still maintained great UV protection abilities.

Conflicts of interest

There are no conflicts to declare.

Acknowledgements

References

1 B. A. Gilchrest, *et al.*, The pathogenesis of melanoma induced by ultraviolet radiation, *N. Engl. J. Med.*, 1999, **340**(17), 1341–1348.

2 G. J. Clydesdale, G. W. Dandie and H. Konrad Muller, Ultraviolet light induced injury: immunological and inflammatory effects, *Immunol. Cell Biol.*, 2001, **79**(6), 547–568.

3 M. Berneburg, H. Plettenberg and J. Krutmann, Photoaging of human skin, *Photodermatol., Photoimmunol. Photomed.*, 2000, **16**(6), 239–244.

4 S. E. Ullrich, Sunlight and skin cancer: lessons from the immune system, *Mol. Carcinog.*, 2007, **46**(8), 629–633.

5 R. P. Sinha and D.-P. Häder, UV-induced DNA damage and repair: a review, *Photochem. Photobiol. Sci.*, 2002, **1**(4), 225–236.

6 F. Aubin, Mechanisms involved in ultraviolet light-induced immunosuppression, *Eur. J. Dermatol.*, 2003, **13**(6), 515–523.

7 S. Scalia, *et al.*, Complexation of the sunscreen agent, phenylbenzimidazole sulphonic acid with cyclodextrins: effect on stability and photo-induced free radical formation, *Eur. J. Pharm. Sci.*, 2004, **22**(4), 241–249.

8 M. Šitum, *et al.*, The role of UV radiation in the development of basal cell carcinoma, *Coll. Antropol.*, 2008, **32**(2), 167–170.

9 J. Roewert-Huber, *et al.*, Epidemiology and aetiology of basal cell carcinoma, *Br. J. Dermatol.*, 2007, **157**, 47–51.

10 P. M. Rodust, *et al.*, UV-induced squamous cell carcinoma – a role for antiapoptotic signalling pathways, *Br. J. Dermatol.*, 2009, **161**, 107–115.

11 K. Morabito, *et al.*, Review of sunscreen and the emergence of non-conventional absorbers and their applications in ultraviolet protection, *Int. J. Cosmet. Sci.*, 2011, **33**(5), 385–390.

12 J. J. Vallejo, M. Mesa and C. Gallardo, Evaluation of the avobenzone photostability in solvents used in cosmetic formulations, *Vitae*, 2011, **18**(1), 63–71.

13 I. Karlsson, *et al.*, Photodegradation of dibenzoylmethanes: potential cause of photocontact allergy to sunscreens, *Chem. Res. Toxicol.*, 2009, **22**(11), 1881–1892.

14 E. Chatelain and B. Gabard, Photostabilization of butyl methoxydibenzoylmethane (avobenzone) and ethylhexyl methoxycinnamate by bis-ethylhexyloxyphenol methoxyphenyl triazine (Tinosorb S), a new UV broadband filter, *Photochem. Photobiol.*, 2001, **74**(3), 401–406.

15 L. Yuan, *et al.*, Studies on the preparation and photostability of avobenzone and (2-hydroxy)propyl-β-cyclodextrin inclusion complex, *J. Photochem. Photobiol., A*, 2019, **369**, 174–180.

16 S. Afonso, *et al.*, Photodegradation of avobenzone: stabilization effect of antioxidants, *J. Photochem. Photobiol., B*, 2014, **140**, 36–40.

17 B. Albertini, *et al.*, Evaluation of spray congealing as technique for the preparation of highly loaded solid lipid microparticles containing the sunscreen agent, avobenzone, *J. Pharm. Sci.*, 2009, **98**(8), 2759–2769.

18 J. Yang, *et al.*, Influence of hydroxypropyl-β-cyclodextrin on transdermal penetration and photostability of avobenzone, *Eur. J. Pharm. Biopharm.*, 2008, **69**(2), 605–612.

19 P.-S. Wu, *et al.*, Effects of the novel poly(methyl methacrylate) (PMMA)-encapsulated organic ultraviolet (UV) filters on the UV absorbance and in vitro sun protection factor (SPF), *J. Photochem. Photobiol., B*, 2014, **131**, 24–30.

20 C. G. Cabrera, *et al.*, Characterization of encapsulation process of avobenzone in solid lipid microparticle using a factorial design and its effect on photostability, *J. Appl. Pharm. Sci.*, 2014, **4**(12), 035–043.

21 S. Scalia, *et al.*, Complexation of the sunscreen agent, butyl-methoxydibenzoylmethane, with hydroxypropyl-β-cyclodextrin, *Int. J. Pharm.*, 1998, **175**(2), 205–213.

22 R. S. Bhuptani and V. B. Patravale, Starch microsponges for enhanced retention and efficacy of topical sunscreen, *Mater. Sci. Eng., C*, 2019, **104**, 109882.

23 Z. Gao, *et al.*, The characterization of organic modified montmorillonite and its filled PMMA nanocomposite, *J. Therm. Anal. Calorim.*, 2001, **64**(2), 467–475.

24 J. R. Philippot, and S. Francis, *Liposomes as tools in basic research and industry*, CRC press, 1994.

25 P. Mura, Analytical techniques for characterization of cyclodextrin complexes in aqueous solution: a review, *J. Pharm. Biomed. Anal.*, 2014, **101**, 238–250.

26 C. J. Brinker, *et al.*, Evaporation-induced self-assembly: nanostructures made easy, *Adv. Mater.*, 1999, **11**(7), 579–585.

27 D. Zhao, *et al.*, Triblock copolymer syntheses of mesoporous silica with periodic 50 to 300 angstrom pores, *science*, 1998, **279**(5350), 548–552.

28 D. Zhao, *et al.*, Nonionic triblock and star diblock copolymer and oligomeric surfactant syntheses of highly ordered, hydrothermally stable, mesoporous silica structures, *J. Am. Chem. Soc.*, 1998, **120**(24), 6024–6036.

29 G. E. Eperon, *et al.*, Morphological control for high performance, solution-processed planar heterojunction perovskite solar cells, *Adv. Funct. Mater.*, 2014, **24**(1), 151–157.

30 M. Colilla, *et al.*, Novel method to enlarge the surface area of SBA-15, *Chem. Mater.*, 2007, **19**(13), 3099–3101.

31 Y. He, *et al.*, Mesoporous silica nanoparticles as potential carriers for enhanced drug solubility of paclitaxel, *Mater. Sci. Eng., C*, 2017, **78**, 12–17.

32 J. M. Palomino, *et al.*, Mesoporous silica nanoparticles for high capacity adsorptive desulfurization, *J. Mater. Chem. A*, 2014, **2**(36), 14890–14895.

33 H. Li, *et al.*, Evaluation of biomimetically synthesized mesoporous silica nanoparticles as drug carriers: structure, wettability, degradation, biocompatibility and brain distribution, *Mater. Sci. Eng., C*, 2019, **94**, 453–464.

34 M. Thommes, Physical adsorption characterization of nanoporous materials, *Chem. Ing. Tech.*, 2010, **82**(7), 1059–1073.

35 K. S. W. Sing, Reporting physisorption data for gas/solid systems with special reference to the determination of surface area and porosity (Recommendations 1984), *Pure Appl. Chem.*, 1985, **57**(4), 603–619.

36 S. Brunauer, *et al.*, On a theory of the van der Waals adsorption of gases, *J. Am. Chem. Soc.*, 1940, **62**(7), 1723–1732.

37 A. R. Abid, *et al.*, Photo-stability and photo-sensitizing characterization of selected sunscreens' ingredients, *J. Photochem. Photobiol., A*, 2017, **332**, 241–250.

38 R. Narayan, *et al.*, Mesoporous silica nanoparticles: a comprehensive review on synthesis and recent advances, *Pharmaceutics*, 2018, **10**(3), 118.

39 C. C. Li, *et al.*, Mesoporous silica aerogel as a drug carrier for the enhancement of the sunscreen ability of benzophenone-3, *Colloids Surf., B*, 2014, **115**, 191–196.

40 V. Trotta, *et al.*, Influence of lipid microparticle encapsulation on in vitro efficacy, photostability and water resistance of the sunscreen agents, octyl methoxycinnamate and butyl methoxydibenzoylmethane, *Drug Dev. Ind. Pharm.*, 2014, **40**(9), 1233–1239.

41 D. R. Hayden, *et al.*, Size and optically tunable ethyl cellulose nanoparticles as carriers for organic UV filters, *ChemNanoMat*, 2018, **4**(3), 301–308.

42 C. Wang, *et al.*, Preparation of rutile TiO_2@avobenzone composites for the further enhancement of sunscreen performance, *RSC Adv.*, 2016, **6**(113), 111865–111871.

43 J. C. Doadrio, *et al.*, Functionalization of mesoporous materials with long alkyl chains as a strategy for controlling drug delivery pattern, *J. Mater. Chem.*, 2006, **16**(5), 462–466.

44 Y.-C. Lin, *et al.*, UV filter entrapment in mesoporous silica hydrogel for skin protection against UVA with minimization of percutaneous absorption, *Eur. J. Pharm. Sci.*, 2018, **122**, 185–194.